Feedback Control for Spacecraft Reorientation Under Attitude Constraints Via Convex Potentials

UNSIK LEE
MEHRAN MESBAHI
University of Washington
Seattle, Washington USA

A novel guidance algorithm is proposed for the attitude reorientation of a rigid body spacecraft in the presence of multiple types of attitude-constrained zones. In this direction, two types of attitude-constrained zones are first developed using unit quaternions, namely, the attitude-forbidden and -mandatory zones. The paper then utilizes a convex parameterization of forbidden and mandatory zones for constructing a strictly convex logarithmic barrier potential that is subsequently used for the synthesis of feedback attitude control laws while the inevitable unwinding phenomenon is given a simple and effective remedy. Model-independent and model-dependent control laws are then implemented by using the Lyapunov direct method and the modified integrator backstepping method. The paper concludes with a set of simulation results to evaluate the effectiveness and demonstrate the viability of the proposed methodology.

Manuscript received April 23, 2012; revised June 2, 2013, September 2, 2013; released for publication January 22, 2014.

DOI. No. 10.1109/TAES.2014.120240.

Refereeing of this contribution was handled by S. Nakasuka.

The research of the authors has been supported by National Science Foundation (Grant No. CMMI-0856737).

Authors' addresses: U. Lee, M. Mesbahi, University of Washington, William E. Boeing Dept. of Aeronautics and Astronautics, Box 352400, Seattle, WA 98195-2400, E-mails: (mesbahi@uw.edu; unsik@uw.edu).

I. NOMENCLATURE

$\mathbf{R}$	set of real numbers
$\mathbf{R}^n$	n-dimensional Euclidean space
$\mathbf{R}_{++}$	set of positive real numbers
$\mathbf{R}_{+}$	set of nonnegative real numbers
$\mathbf{S}^n$	set of $n \times n$ symmetric matrices
$\mathbf{S}^n_{++}$	set of $n \times n$ positive definite matrices
SO(3)	special orthogonal group of three dimensions
$\boldsymbol{I}_n$	n-dimensional identity matrix
$\mathbf{0}_{n\times m}$	$n \times m$ zero matrix
$\mathbf{q}$	unit quaternion; $\mathbf{q} = [\boldsymbol{q}^T q_0]^T$
$\mathbf{q}^*$	quaternion conjugate; $\mathbf{q} = [-\boldsymbol{q}^T q_0]^T$
$\boldsymbol{q}$	vector part of the unit quaternion $\mathbf{q}$
q_0	scalar part of the unit quaternion $\mathbf{q}$
$\mathbf{q}_{\mathrm{I}}$	identity unit quaternion $\mathbf{q}_{\mathbf{I}} = [0\ 0\ 0\ 1]^T$
$\mathbf{q}_{\boldsymbol{d}}$	desired attitude in unit quaternion
$\mathbf{U}_{\mathrm{q}}$	set of unit quaternions
$\mathbf{Q}_{\boldsymbol{F}}$	complement of attitude-forbidden zone
$\mathbf{Q}_{\boldsymbol{M}}$	set of attitude-mandatory zone
$\mathbf{Q}_{\boldsymbol{P}}$	set of attitude-permissible zone
∂D	boundary of the set D
$\boldsymbol{x} \cdot \boldsymbol{y}$	dot product between vectors $\boldsymbol{x}$ and $\boldsymbol{y}$
$\otimes$	quaternion multiplication
$\boldsymbol{\omega}$	angular velocity vector in the body frame
$R(\boldsymbol{\omega})$	cross product operator associated with $\boldsymbol{\omega}$
$\tilde{\boldsymbol{\omega}}$	angular velocity in quaternion form; $\tilde{\boldsymbol{\omega}} = [\boldsymbol{\omega}^T 0]^T$
$\|x\|$	Euclidean two-norm of vector or quaternion x
Diag(x)	diagonal matrix with vector x on its diagonal
Vec[$\cdot$]	3×1 vector part of the argument

II. INTRODUCTION

The execution of large-angle reorientation of spacecraft while avoiding unwanted celestial objects is one of the challenging but desirable technologies for spacecraft autonomy. This type maneuvering occurs quite often in actual spacecraft missions. For example, spacecraft involved in science missions are often equipped with sensitive payloads, such as infrared telescopes or interferometers, that require retargeting while keeping away from direct exposure to the sunlight or other bright objects. This requirement is often accompanied by additional requirements on other spacecraft instruments. For example, a nonarticulated high-gain antenna for communication with ground stations requires that the spacecraft attitude remains in a particular cone during the spacecraft maneuver. Another example is spacecraft cross-link communication in formation flying; in this case, retaining the ability to reorient the spacecraft while also pointing the antennas toward the neighboring spacecraft provides a number of advantages over requiring expensive, high-power omnidirectional antennas [1]. Planning a reorientation in the presence of attitude-constrained zones is of paramount importance in such science missions; it also poses a challenging computational task for the spacecraft guidance, navigation, and control subsystem.

The fundamental complexity of such problems is mainly because rotational configuration space SO(3) is a boundaryless compact manifold, from which removing the constrained zones results in a nonconvex region.

The spacecraft reorientation problem in the absence of attitude-constrained zones has been comprehensively addressed in nonlinear control literature [2–9]. For instance, backstepping [8–10], sliding mode control [7], adaptive control [5, 6], and the optimal control framework [11–13], have been applied to this problem over the past few decades. In particular, unit quaternion-based control laws have received particular attention because the unit quaternion is the minimal globally singular–free representation of the rigid body's attitude (e.g., see [10, 14–17]). On the contrary, the attitude reorientation problem in the presence of attitude-constrained zones has been examined in only a few research works. For example, McInnes considered and implemented maneuver planning in the presence of attitude-constrained zones via an artificial potential function in [18–20]. However, because of the use of Euler angles in McInnes' works, the possibility of having singularities during reorientation maneuvers could not be ruled out. Another set of approaches to constrained attitude control, which relies on geometric relations between the direction of the instrument's boresight and the bright celestial object to be avoided, has been introduced by Spindler [21], Hablani [22], and Frakes et al. [23]. In these research works, a feasible attitude trajectory is determined before the reorientation maneuver and generated on the basis of the geometric relations with the exclusion zones. These approaches have a disadvantage of not being extendible to more complex situations, involving multiple celestial constrained zones, as often encountered in space missions. Over the last decade, alternative approaches using randomized algorithms have also been proposed by Frazzoli et al. [24], Kornfeld [25], and Cui et al. [26] to constrained-motion planning problems. The randomization-based approaches have an advantage in terms of their ability to handle distinct classes of constraints, with provable—albeit probabilistic—convergence properties. The randomized algorithms, however, have limitations in terms of their on-board implementation and might result in execution times that, depending on the types of constrained zones and initial and final attitudes, can be of exponential order. Recently, Koenig [1] proposed an algorithm that alters the boresight pointing direction, rotating it by some angle in a normal direction to that of the rate command, and Kjellberg and Lightsey [27] presented a discretized pathfinding algorithm through the pixelization of the configuration space.

In the meantime, Kim and Mesbahi [28, 29] proposed the quaternion-based convex attitude constraint parameterization that builds on the constraint set representation discussed in [30]. In this paper, we expand upon the results of [28, 29] to propose a potential function–based approach to constrained attitude control over more general constrained sets. The advantage of the proposed approach hinges on the fact that the logarithmic barrier potential used for constructing the corresponding control law is smooth and strictly convex. This in turn implies that the proposed methodology can simultaneously handle large numbers of forbidden and mandatory zones, while guaranteeing computational tractability and guaranteed convergence. Subsequently, two types of feedback control laws for constrained reorientation problem are derived in this paper. These feedback controllers will be referred to as model independent and model dependent. In this direction, the model-independent control law is first derived from an energy-based Lyapunov function [28]. The model-dependent control law, on the other hand, is obtained by the modified backstepping method. The backstepping method has been favored by a number of researchers because of the cascade structure of attitude dynamics. In this paper, we adopt the modified backstepping method introduced in [8] to avoid excessive control torque commands during the initial phase of the reorientation maneuver.

The rest of the paper is organized as follows: Section III reviews the mathematical models of rigid-body kinematics and dynamics using quaternions and then briefly discusses a solution for the unwinding phenomenon that is used for our simulation results. In Section IV, we define and parameterize two classes of attitude-constrained zones. These zones are then convexified and embedded in the corresponding logarithmic barrier potential for the synthesis of constrained attitude maneuver control in Section V. Two control design techniques for constrained attitude maneuver are then presented in Section VI, followed by three simulation scenarios examined in Section VII. Conclusions and future extensions of this work are detailed in Section VIII.

III. PRELIMINARIES

The attitude of a rigid spacecraft, describing its relative orientation between a reference frame and the body fixed frame, evolves on the special orthogonal group SO(3). In this work, we will be utilizing the unit quaternion representation to parameterize SO(3). The state space of unit quaternions $\mathbf{U_q}$ forms a boundaryless compact manifold in SO(3), where

$$\mathbf{U_q} = \{\mathbf{q} \in \mathbf{R}^4 \mid \|\mathbf{q}\| = 1\}. \tag{1}$$

A unit quaternion is defined as $\mathbf{q} = [\boldsymbol{q}^T q_0]^T \in \mathbf{U_q}$, where $\boldsymbol{q} = \hat{\mathbf{n}} \sin\left(\frac{\phi}{2}\right) \in \mathbf{R}^3$ denotes the vector part of the quaternion, and $q_0 = \cos\left(\frac{\phi}{2}\right) \in \mathbf{R}$ denotes its scalar part; $\hat{\mathbf{n}}$ and ϕ refer to, respectively, the Euler axis and the rotation angle about this axis corresponding to the rigid body orientation. We adopt the notation "$\otimes$" for quaternion multiplication defined by

$$\mathbf{q} \otimes \mathbf{p} = \begin{bmatrix} q_0 \boldsymbol{p} + p_0 \boldsymbol{q} + \boldsymbol{q} \times \boldsymbol{p} \\ q_0 p_0 - \boldsymbol{q}^T \boldsymbol{p} \end{bmatrix}, \tag{2}$$

where $\mathbf{q} = [\boldsymbol{q}^T, q_0]^T$ and $\mathbf{p} = [\boldsymbol{p}^T, p_0]^T$. Another quaternion operation is the quaternion conjugate defined as $\mathbf{q}^* = [-\boldsymbol{q}^T q_0]^T$, which facilitates the judicious definition for attitude difference/error of $\mathbf{p}$ with respect to $\mathbf{q}$ via

$$\mathbf{q}^* \otimes \mathbf{p} = \begin{bmatrix} q_0\boldsymbol{p} - p_0\boldsymbol{q} - \boldsymbol{q} \times \boldsymbol{p} \\ q_0 p_0 + \boldsymbol{q}^T \boldsymbol{p} \end{bmatrix}, \tag{3}$$

where $\mathbf{q}$, $\mathbf{p}$, and $\mathbf{q}^* \otimes \mathbf{p} \in \mathbf{U_q}$. Given the attitude $\mathbf{q}$, the position vector $\boldsymbol{y}$ in body coordinates can be represented in the inertial coordinates as

$$\boldsymbol{y}' = \mathbf{q} \otimes \boldsymbol{y} \otimes \mathbf{q}^*, \tag{4}$$

where $\boldsymbol{y}'$ denotes the position vector expressed in the inertial coordinates. We note here that (4) can also be interpreted as the rotation $\mathbf{q}$ of the vector $\boldsymbol{y}$. When quaternions are represented as elements in $\mathbf{R}^4$, their algebraic properties can be extended with respect to vector-based products such as the inner product. The following are some of these extended algebraic properties of quaternions:

$$\mathbf{a} \otimes (\mathbf{b} + \mathbf{c}) = \mathbf{a} \otimes \mathbf{b} + \mathbf{a} \otimes \mathbf{c} \tag{5}$$

$$(\mathbf{a} \otimes \mathbf{b})^* = \mathbf{b}^* \otimes \mathbf{a}^* \tag{6}$$

$$(\gamma \mathbf{a}) \otimes \mathbf{b} = \mathbf{a} \otimes (\gamma \mathbf{b}) = \gamma(\mathbf{a} \otimes \mathbf{b}) \tag{7}$$

$$\mathbf{a} \otimes (\mathbf{b} \otimes \mathbf{c}) = (\mathbf{a} \otimes \mathbf{b}) \otimes \mathbf{c} \tag{8}$$

$$\mathbf{a}^T(\mathbf{b} \otimes \mathbf{c}) = c^T(\mathbf{b}^* \otimes \ \mathbf{a}) = \mathbf{b}^T(\mathbf{a} \otimes \mathbf{c}^*), \tag{9}$$

where $\gamma \in \mathbf{R}$. In particular, (9) will subsequently be used in the derivation of feedback control laws for constrained motion planning.

The unit quaternion is globally nonsingular in representing an attitude on SO(3) [32]. The potential function

$$V_I : \mathbf{U_q} \to \mathbf{R}_+$$

for attitude regulation to the identity quaternion can be defined as

$$V_I = \|\mathbf{q} - \mathbf{q_I}\|^2, \tag{10}$$

which leads to a Lyapunov function about $\mathbf{q_I}$ along the rigid body kinematics, leading to a stabilizing control law.

PROPOSITION 1 Let $\mathbf{q} \in \mathbf{U_q}$. Then

$$\left\|\mathbf{q}_d^* \otimes \mathbf{q} \pm \mathbf{q_I}\right\|^2 = \|\mathbf{q}_d \pm \mathbf{q}\|^2, \tag{11}$$

where $\mathbf{q}_d$ denotes the desired attitude.

PROOF The proof follows by utilizing the properties of unit quaternions as

$$\begin{aligned} \left\|\mathbf{q}_d^* \otimes \mathbf{q} \pm \mathbf{q_I}\right\|^2 &= 2 \pm 2\mathbf{q}_\mathbf{I}^T(\mathbf{q}_d^* \otimes \mathbf{q}) \\ &= 2 \pm 2\mathbf{q}_d^T\mathbf{q} \\ &= \mathbf{q}_d^T\mathbf{q}_d + \mathbf{q}^T\mathbf{q} \pm 2\mathbf{q}_d^T\mathbf{q} \\ &= \|\mathbf{q}_d \pm \mathbf{q}\|^2, \end{aligned}$$

which employs the identity $(\mathbf{q}_d^* \otimes \mathbf{q})^T(\mathbf{q}_d^* \otimes \mathbf{q}) = 1$. ■

A direct consequence of Proposition 1 is that the function $V_I(10)$ defines a quaternion error potential function with respect to the identity quaternion.

The unit quaternion inherently possesses a sign ambiguity; for example, $\frac{1}{2}\pi$ rotation and $-\frac{3}{2}\pi$ rotation about the same eigenaxis geometrically represent the same attitude on SO(3) but correspond to two distinct unit quaternions, say $\mathbf{q}$ and $-\mathbf{q}$. This ambiguity leads to having two choices for an identity quaternion in the attitude space, namely $\mathbf{q_I}$ and $-\mathbf{q_I}$. For example, a feedback control designed with a poorly chosen sign for the identity quaternion with a large initial attitude error ($\phi \geq \pi$) might not lead to a desirable trajectory on SO(3), exhibiting the so-called "unwinding" behavior [33], where the reorientation trajectory is nongeodesic. This is because the unit quaternion is a boundaryless compact manifold that doubly covers SO(3). Recently, Christopher et al. [34, 35] have presented a path-lifting mechanism for avoiding the unwinding phenomenon, whereas Han et al. [36] have proposed an analogous approach with dual quaternions. A simple remedy to avoid the unwinding behavior, subsequently used in Section VII, is also outlined below.

In subsequent sections, we will utilize an attitude error function $V : \mathbf{U_q} \times \mathbf{U_q} \to \mathbf{R}_+$, measuring the error between the current attitude and the desired attitude as

$$V = \left\|\mathbf{q}_d^\star \otimes \mathbf{q} \pm \mathbf{q_I}\right\|^2 = \|\mathbf{q}_d \pm \mathbf{q}\|^2, \tag{12}$$

where $\mathbf{q}_d$ denotes the desired attitude and $\pm$ denotes the sign that will be chosen depending on the sign of $\mathbf{q_I}$.

PROPOSITION 2 Consider the function (12) as a Lyapunov function candidate with an initial (error) attitude

$$\mathbf{q}_d^\star \otimes \mathbf{q}_0 = \left[\hat{n}^T \sin\frac{\phi}{2} \cos\frac{\phi}{2}\right]^T \in \mathbf{U_q}, \tag{13}$$

where $\mathbf{q}_0$ denotes the initial attitude. Then, following the negative gradient of V and selecting the identity quaternion $\mathbf{q_I}$ to have the opposite sign as $\cos\frac{\phi}{2}$, the scalar part of $\mathbf{q}_d^\star \otimes \mathbf{q}_0$, leads to a rotation with an angle less than or equal to π about the corresponding eigenaxis. In other words, the sign of $\mathbf{q_I}$ can be chosen such that the corresponding rotation on SO(3) traverses an angle less than π.

PROOF The candidate Lyapunov function in (12) includes a component associated with the scalar part of the unit quaternion as

$$V_s = \|q_0 \pm 1\|^2 = \left\|\cos\frac{\phi}{2} \pm 1\right\|^2, \quad \text{for all } \phi, \tag{14}$$

where q_0 denotes the scalar part of $\mathbf{q}_d^\star \otimes \mathbf{q}_0$, ϕ denotes the rotation angle about the eigenaxis $\hat{n}$, and ± 1 corresponds to the selection of the identity quaternion as $\mathbf{q_I} = [0\ 0\ 0\ 1]$ or $-\mathbf{q_I} = [0\ 0\ 0\ -1]$. Choosing the identity quaternion with the sign opposite $\cos\frac{\phi}{2}$, (14) translates to an equivalent

form

$$V_s' = \left\| \cos\frac{\phi'}{2} - 1 \right\|^2, \quad -\pi < \phi' \leq \pi, \tag{15}$$

which is strictly convex in ϕ'. We now note that V_s' monotonically decreases as ϕ' approaches zero. For example, the rotation angle $\phi = \frac{5}{4}\pi$ with the selection of $\mathbf{q_I} = [0\ 0\ 0\ 1]$ leads to

$$V_s = \left\| \cos\frac{\phi}{2} + 1 \right\|^2 = \left\| \cos\frac{\phi'}{2} - 1 \right\|^2, \tag{16}$$

where $\phi' = \pm\frac{1}{4}\pi$. Thus, following the negative gradient of V_s leads to a geodesic trajectory toward the desired attitude, avoiding the unwinding phenomenon. ■

As suggested by Proposition 2, in this paper we will select the identity unit quaternion $\mathbf{q_I}$, representing the origin in the attitude space, to have a sign opposite the scalar part of $\mathbf{q}_d^\star \otimes \mathbf{q}$ to avoid the unwinding phenomenon.

A. Rigid-Body Dynamics

Before delving into the main topic of the present paper, let us briefly review fundamentals of rigid-body dynamics [37]. The attitude dynamics of a rigid spacecraft equipped with fully actuated body-fixed torque generating devices can be described as,

$$\dot{\mathbf{q}}(t) = \frac{1}{2}\mathbf{q}(t) \otimes \tilde{\boldsymbol{\omega}}(t), \tag{17}$$

$$J\dot{\boldsymbol{\omega}}(t) = R(\boldsymbol{\omega})J\boldsymbol{\omega}(t) + \boldsymbol{u}(t), \tag{18}$$

where $\mathbf{q}(t)$ is the unit quaternion representing the attitude of the rigid body at time t, $\boldsymbol{\omega}(t) \in \mathbf{R}^3$denotes the angular velocity of the spacecraft in the body frame, $\tilde{\boldsymbol{\omega}}(t) = [\boldsymbol{\omega}^T\ 0]^T_{4\times 1}$, $J = \mathrm{Diag}(J_1, J_2, J_3)$ denotes the inertia matrix of the spacecraft in the body frame, $\boldsymbol{u}(t) \in \mathbf{R}^3$ represents the control torques about the body axes, and $R(\boldsymbol{\omega})$ denotes the negative cross-product operator in the matrix form associated with $\boldsymbol{\omega}$ given as

$$R(\boldsymbol{\omega}) = \begin{bmatrix} 0 & \omega_3 & -\omega_2 \\ -\omega_3 & 0 & \omega_1 \\ \omega_2 & -\omega_1 & 0 \end{bmatrix}. \tag{19}$$

In this paper, to focus on deriving reorientation control laws for constrained-attitude maneuvers, we assume that all external disturbances on the spacecraft are negligible.

IV. ATTITUDE-CONSTRAINED ZONES

In this section, we define three types of attitude-constrained zones that will be the focus of our discussion in this paper:

1) *Attitude-Forbidden Zone*: A set of spacecraft orientations, such as the set of attitudes that lead the sensitive on-board instruments to have a direct exposure to certain celestial objects (e.g., the sun) is considered an attitude-forbidden zone. Multiple constrained zones can be specified with respect to a single instrument boresight vector.

2) *Attitude-Mandatory Zone*: A set of spacecraft orientations, such as the set of attitudes that lead certain on-board instruments to point toward specified objects (e.g., pointing a high gain antenna to a ground station) is considered an attitude-mandatory zone. The attitude-mandatory zones for each instrument should be nonconflicting.

3) *Attitude-Permissible Zone*: A set of spacecraft orientations is considered an attitude-permissible zone when it is at the intersection of the complements of attitude-forbidden zones on one hand and the attitude-mandatory zones on the other.

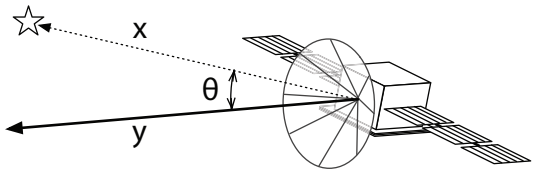

Fig. 1. Maintaining minimum angle of θ between boresight vector y in body frame and inertial vector x.

Suppose an angle strictly greater than θ should be maintained between the normalized boresight vector y of the spacecraft instrument and the normalized vector x pointing toward a certain celestial object, as shown in Fig. 1. This requirement can be expressed as

$$\boldsymbol{x} \cdot \boldsymbol{y}' < \cos\theta, \tag{20}$$

where

$$\begin{aligned} \boldsymbol{y}' &= \mathbf{q} \otimes \boldsymbol{y} \otimes \mathbf{q}^* \\ &= \boldsymbol{y} - 2(\boldsymbol{q}^T\boldsymbol{q})\boldsymbol{y} + 2(\boldsymbol{q}^T\boldsymbol{y})\boldsymbol{q} + 2q_0(\boldsymbol{y}\times\boldsymbol{q}) \end{aligned} \tag{21}$$

denotes the instrument's boresight vector represented in the inertial coordinates, taking into account the spacecraft attitude $\mathbf{q}$. Note that the position vector $\mathbf{x}$ is represented in the inertial coordinates. Combining (20) and (21) yields

$$2\boldsymbol{q}^T\boldsymbol{y}\boldsymbol{q}^T\boldsymbol{x} - \boldsymbol{q}^T\boldsymbol{q}\boldsymbol{x}^T\boldsymbol{y} + q_0^2\boldsymbol{x}^T\boldsymbol{y} + 2q_0\boldsymbol{q}^T(\boldsymbol{x}\times\boldsymbol{y}) < \cos\theta. \tag{22}$$

After some algebraic manipulations, we thus obtain [31, 38]

$$\mathbf{q}^T\begin{bmatrix} A & b \\ b^T & d \end{bmatrix}\mathbf{q} < 0, \tag{23}$$

where

$$\begin{aligned} A &= \boldsymbol{x}\boldsymbol{y}^T + \boldsymbol{y}\boldsymbol{x}^T - (\boldsymbol{x}^T\boldsymbol{y} + \cos\theta)\mathbf{I}_3, \\ b &= \boldsymbol{x}\times\boldsymbol{y}, \quad d = \boldsymbol{x}^T\boldsymbol{y} - \cos\theta. \end{aligned} \tag{24}$$

Such a representation, on the other hand, enables the parameterization of the three aforementioned constrained zones into the form of quadratic inequalities, as we proceed to show below.

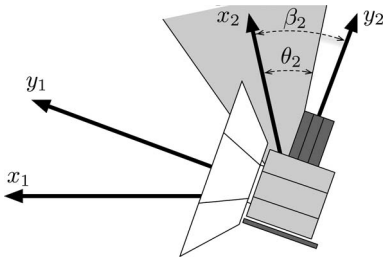

Fig. 2. Attitude-forbidden zone associated with instrument boresight vector $\boldsymbol{y}_2$.

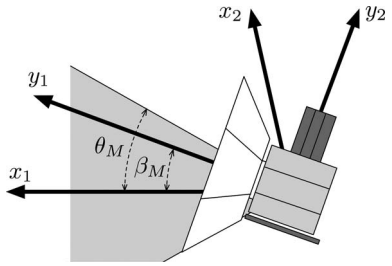

Fig. 3. Attitude-mandatory zone associated with instrument boresight vector $\boldsymbol{y}_1$.

A. Complement of Attitude-Forbidden Zones

Consider the spacecraft attitude $\mathbf{q} \in \mathbf{U_q}$ for which the boresight vector $\boldsymbol{y_j}$ for the jth instrument (e.g., a telescope) lies outside of the attitude-forbidden zone (i.e., $\beta_2 > \theta_2$ in Fig. 2). The set of such orientations $\mathbf{Q}_{\boldsymbol{F}_i^j} \subseteq \mathbf{U_q}$ can be represented as,

$$\mathbf{Q}_{\boldsymbol{F}_i^j} = \{\mathbf{q} \in \mathbf{U_q} \mid \mathbf{q}^T M_i^j(\theta_i^j)\mathbf{q} < 0\}, \tag{25}$$

with

$$M_i^j(\theta_i^j) = \begin{bmatrix} A_i^j & b_i^j \\ b_i^{jT} & d_i^j \end{bmatrix}, \tag{26}$$

where

$$A_i^j = \boldsymbol{x}_i \boldsymbol{y}_j^T + \boldsymbol{y}_j \boldsymbol{x}_i^T - (\boldsymbol{x}_i^T \boldsymbol{y}_j + \cos\theta_i^j) I_3, \tag{27}$$

$$b_i^j = \boldsymbol{x}_i \times \boldsymbol{y}_j, \qquad d_i^j = \boldsymbol{x}_i^T \boldsymbol{y}_j - \cos\theta_i^j,$$
$$i = 1, 2, \ldots, n, \quad j = 1, 2, \ldots, m. \tag{28}$$

Let us elaborate on the notation used above. The index i represents the number of constrained objects associated with the jth on-board instrument; the index j, on the other hand, is the number of instruments. Thus M_i^j corresponds to the ith celestial object and the jth instrument. Moreover, $\boldsymbol{x}_i$ denotes the unit vector (specified in the inertial frame) for the ith constrained object to be avoided, whereas $\boldsymbol{y}_j$ indicates the unit vector (in the body frame) representing the boresight direction of the jth sensitive instrument on the spacecraft. The angle θ_i^j is the constraint angle about the direction of the ith object specified by $\boldsymbol{x}_i$ for the jth instrument boresight vector $\boldsymbol{y}_j$. Without loss of generality, the domain of the angle θ_i^j for all i, j is restricted to be $(0, \pi)$. We note that an attitude-forbidden zone with $\theta_i^j \geq \frac{1}{2}\pi$ represents the same attitude-constrained zone on the celestial sphere as the attitude-mandatory zone with an angle $\pi - \theta_i^j$. The attitude-forbidden zone is generally defined not only with respect to the number of on-board sensitive instruments m, but also with respect to the number of constraint objects n.

B. Attitude-Mandatory Zone

The set $\mathbf{Q}_{\boldsymbol{M}} \subseteq \mathbf{U_q}$ represents possible attitudes of the spacecraft on which the boresight vector of an on-board instrument (e.g., an antenna) lies inside the attitude-mandatory zone (i.e., $\beta_M < \theta_M$ in Fig. 3). This set can be represented as

$$\mathbf{Q}_{\boldsymbol{M}} = \{\mathbf{q} \in \mathbf{U_q} \mid \mathbf{q}^T M_M(\theta_M)\mathbf{q} > 0\}, \tag{29}$$

where $M_M(\theta_M)$ and θ_M are defined analogous to (26), with respect to the boresight vector of an on-board instrument, which should stay in the attitude-mandatory zone. The angle θ_M in (29) is the constraint angle for the attitude-mandatory zone about the direction of the object specified by $\boldsymbol{x}_1$ in Fig. 3. Note that we have considered the case where only one attitude-mandatory zone is present; this is without loss of generality, as if multiple mandatory zones are present, only the set defined by their intersection can be considered.

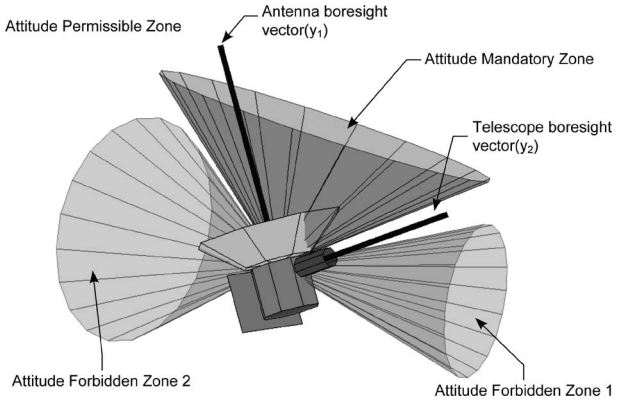

Fig. 4. Three types of constrained zones shown on celestial space. Attitude-mandatory zone is associated with antenna boresight vector y_1; telescope boresight vector y_2 is associated with attitude-forbidden zones 1 and 2.

C. Attitude-Permissible Zone

Let us also provide a representation for the attitude-permissible zone. The subset $\mathbf{Q}_{\boldsymbol{P}}$, parameterizing the attitude of the spacecraft satisfying the attitude-mandatory zones, as well as avoiding the attitude-forbidden zones, is given by

$$\mathbf{Q}_{\boldsymbol{P}} = \{\mathbf{q} \in \mathbf{U_q} \mid \mathbf{q} \in \mathbf{Q}_{\boldsymbol{F}_i^j} \text{ and } \mathbf{q} \in \mathbf{Q}_{\boldsymbol{M}}\},$$
$$i = 1, 2, \ldots, n, \ j = 1, 2, \ldots, m. \tag{30}$$

Fig. 4 depicts three types of attitude-constrained zones shown on the celestial sphere and defined with respect to two instrument boresight vectors $\boldsymbol{y}_1$ and $\boldsymbol{y}_2$.

V. PROBLEM STATEMENT

We now consider the problem of designing feedback control laws of the form $u = f(\mathbf{q}, \boldsymbol{\omega})$, such that $\mathbf{q} \to \mathbf{q}_d$ and $\boldsymbol{\omega} \to \mathbf{0}$, where $\mathbf{q}_d$ denotes the desired attitude, while guaranteeing that $\mathbf{q}(t) \in \mathbf{Q}_P$ for all $t \geq 0$, where $\mathbf{Q}_P$ denotes the attitude-permissible zone.

We first provide the necessary observations that will be subsequently used for the convex parameterization of the forbidden and mandatory zones and their respective embedding in a potential function.

PROPOSITION 3 Let $M(\theta)$ be the matrix used in the representation of the complement of attitude-forbidden zones in (25). Then, for $\theta \in (0, \pi)$, one has

$$-2 < \lambda_{\min}(M) \leq \mathbf{q}^T M \mathbf{q} \leq \lambda_{\max}(M) < 2. \tag{31}$$

PROOF From (26), the symmetric matrix $M(\theta)$ can be written

$$M(\theta) = P - \cos\theta \mathbf{I}_4, \tag{32}$$

where

$$P = \begin{bmatrix} \boldsymbol{x}\boldsymbol{y}^T + \boldsymbol{y}\boldsymbol{x}^T - (\boldsymbol{x}^T\boldsymbol{y})\mathbf{I}_3 & \boldsymbol{x} \times \boldsymbol{y} \\ (\boldsymbol{x} \times \boldsymbol{y})^T & \boldsymbol{x}^T\boldsymbol{y} \end{bmatrix}. \tag{33}$$

Since vectors $\boldsymbol{x}$ and $\boldsymbol{y}$ are unit vectors, $P^TP = \mathbf{I}_4$. Thus,

$$\begin{aligned} P\boldsymbol{v} &= \lambda_p \boldsymbol{v} \\ P^T P\boldsymbol{v} &= \lambda_p P\boldsymbol{v}, \\ \left(\mathbf{I}_4 - \lambda_p^2\right)\boldsymbol{v} &= 0, \end{aligned}$$

where λ_p is an eigenvalue of P, and $\boldsymbol{v}$ is the corresponding eigenvector. The eigenvalues of P, on the other hand, are

$$\lambda_p = -1,\ -1,\ 1,\ 1. \tag{34}$$

Note that from (32), eigenvalues of the matrix $M(\theta)$ are shifted from λ_p by $\cos\theta$, which assumes values between -1 and 1. Therefore, in view of the fact that $\|\mathbf{q}(t)\| = 1$, (31) follows. ■

PROPOSITION 4 Let $M_i^j(\theta_i^j)$ be the matrix employed to represent the complement of attitude-forbidden zones in (25). Consider the corresponding quaternion subset $\boldsymbol{Q}_{F_i^j} \subseteq \mathbf{U}_\mathbf{q}$ specified as

$$\mathbf{Q}_{\boldsymbol{F}_i^j} = \{\mathbf{q} \in \mathbf{U}_\mathbf{q} \mid \mathbf{q}^T M_i^j(\theta_i^j)\mathbf{q} < 0\}. \tag{35}$$

Then this set can be represented as a convex set

$$\mathbf{Q}'_{\boldsymbol{F}_i^j} = \{\mathbf{q} \in \mathbf{U}_\mathbf{q} \mid \mathbf{q}^T \tilde{M}_i^j(\theta_i^j)\mathbf{q} < 2\}, \tag{36}$$

where $\tilde{M}_i^j(\theta) \in \mathbf{S}^4_{++}$.

PROOF The proof is inspired by an analogous argument presented in [30]. From (31) in Proposition 3, it follows that

$$\begin{aligned} &-2 < \lambda_{\min}(M_i^j(\theta_i^j)) \leq \mathbf{q}^T M_i^j(\theta_i^j)\mathbf{q} < 0, \\ &0 < \lambda_{\min}(M_i^j(\theta_i^j)) + 2 \leq \mathbf{q}^T M_i^j(\theta_i^j)\mathbf{q} + 2 < 2, \\ &0 < \lambda_{\min}(M_i^j(\theta_i^j)) + 2 \leq \mathbf{q}^T M_i^j(\theta_i^j)\mathbf{q} + 2\mathbf{q}^T\mathbf{q} < 2, \\ &0 < \lambda_{\min}(M_i^j(\theta_i^j)) + 2 \leq \mathbf{q}^T (M_i^j(\theta_i^j) + 2\mathbf{I}_4)\mathbf{q} < 2, \\ &0 < \lambda_{\min}(M_i^j(\theta_i^j)) + 2 \leq \mathbf{q}^T \tilde{M}_i^j(\theta_i^j)\mathbf{q} < 2, \\ &0 < \mathbf{q}^T \tilde{M}_i^j(\theta_i^j)\mathbf{q} < 2, \end{aligned}$$

where $\mathbf{q}^T\mathbf{q} = 1$ and $\tilde{M}_i^j(\theta_i^j) \in \mathbf{S}^4_{++}$. Therefore, the subsets $\mathbf{Q}_{\boldsymbol{F}_i^j}$ and $\mathbf{Q}'_{\boldsymbol{F}_i^j}$ above represent the same convex set. ■

PROPOSITION 5 Analogous to Proposition 4, let $M_M(\theta) \in \mathbf{S}^4$ be the matrix in the representation (29). Then the subset $\mathbf{Q}_M \subseteq \mathbf{U}_\mathbf{q}$ specifying the attitude-mandatory zone

$$\mathbf{Q}_M = \{\mathbf{q} \in \mathbf{U}_\mathbf{q} \mid 0 < \mathbf{q}^T M_M(\theta)\mathbf{q}\} \tag{37}$$

can be represented as a convex set

$$\mathbf{Q}'_M = \{\mathbf{q} \in \mathbf{U}_\mathbf{q} | \mathbf{q}^T \tilde{M}_M(\theta)\mathbf{q} < 2\}, \tag{38}$$

where $\tilde{M}_M(\theta) \in \mathbf{S}^4_{++}$.

PROOF The proof follows by observing the following inequalities,

$$\begin{aligned} &0 < \mathbf{q}^T M_M(\theta)\mathbf{q} \leq \lambda_{\max}(M(\theta)) < 2 \\ &-2 < \mathbf{q}^T M_M(\theta)\mathbf{q} - 2 \leq \lambda_{\max}(M(\theta)) - 2 < 0, \\ &-2 < -\mathbf{q}^T \tilde{M}_M(\theta)\mathbf{q} \leq \lambda_{\max}(M(\theta)) - 2 < 0, \\ &0 < -\lambda_{\max}(M(\theta)) + 2 \leq \mathbf{q}^T \tilde{M}_M(\theta)\mathbf{q} < 2, \end{aligned}$$

where $\mathbf{q}^T\mathbf{q} = 1$ and $\tilde{M}_M \in \mathbf{S}^4_{++}$. Hence, the two subsets $\mathbf{Q}_M$ and $\mathbf{Q}'_M$ above represent the same convex set. ■

To utilize the convex parameterization of the forbidden and mandatory zones in the context of a potential function, we consider a logarithmic barrier function $V : \mathbf{Q}_P \to \mathbf{R}$,

$$V(\mathbf{q}) = \|\mathbf{q}_d - \mathbf{q}\|^2 \Bigg[\underbrace{\sum_{j=1}^{m}\sum_{i=1}^{n} -k_1 \log\left(-\frac{\mathbf{q}^T M_i^j \mathbf{q}}{2}\right)}_{\text{attitude-forbidden zones}} \underbrace{-k_2 \log\left(\frac{\mathbf{q}^T M_M \mathbf{q}}{2}\right)}_{\text{attitude-mandatory zone}} \Bigg], \tag{39}$$

where $\mathbf{Q}_P \subseteq \mathbf{U}_\mathbf{q}$, k_1 and k_2 are positive weighting parameters for the attitude-forbidden and -mandatory zones, respectively, and $\mathbf{q}_d$ is the desired attitude. We note that the notational dependency of the matrices M_i^j and M_M on the angle θ_i^j has been suppressed above; we will continue to use this shortened notation in the reminder of our discussion.

PROPOSITION 6 The potential function V defined by (39) is smooth and strictly convex for all $\mathbf{q} \in \mathbf{Q}_P$ and admits a global minimum at $\mathbf{q}_d \in \mathbf{Q}_P$.

PROOF We will show that V in (39) meets the following three conditions:

1) $V(\mathbf{q}_d) = 0$,
2) $V(\mathbf{q}) > 0$, for all $\mathbf{q} \in \mathbf{Q}_P \setminus \{\mathbf{q}_d\}$
3) $\nabla^2 V(\mathbf{q})$ is positive definite for all $\mathbf{q} \in \mathbf{Q}_P$.

It is clear that $V(\mathbf{q}_d) = 0$. From (35) and (37), the inequalities

$$0 < -\frac{\mathbf{q}^T M_i^j \mathbf{q}}{2} < 1 \text{ and } 0 < \frac{\mathbf{q}^T M_M \mathbf{q}}{2} < 1 \tag{40}$$

hold; hence, the negative logarithm function (39) is always positive; moreover, for all $\mathbf{q} \in \mathbf{Q}_P$,

$$\sum_{i=1}^{n} -\log\left(-\frac{\mathbf{q}^T M_i^j \mathbf{q}}{2}\right) > 0 \text{ and } -\log\left(\frac{\mathbf{q}^T M_M \mathbf{q}}{2}\right) > 0. \tag{41}$$

Hence $V(\mathbf{q}) > 0$ for all $\mathbf{q} \in \mathbf{Q}_P \backslash \{\mathbf{q}_d\}$.

The last part of the proposition can be shown by first swapping the quaternion quadratic terms $-\mathbf{q}^T M_i^j \mathbf{q}$ and $\mathbf{q}^T M_M \mathbf{q}$ for the following equivalent terms:

$$\begin{aligned} -\mathbf{q}^T M_i^j \mathbf{q} &> 0, \\ -\mathbf{q}^T M_i^j \mathbf{q} + \beta_1 - \beta_1 &> 0, \\ \mathbf{q}^T \tilde{M}_i^j \mathbf{q} - \beta_1 &> 0, \end{aligned} \tag{42}$$

where β_1 is defined as $-\lambda_{\max}(M_i^j) + \beta_1 > 0$ such that $\tilde{M}_i^j$ is a positive definite matrix, and

$$\begin{aligned} \mathbf{q}^T M_M \mathbf{q} &> 0, \\ \mathbf{q}^T M_M \mathbf{q} + \beta_2 - \beta_2 &> 0, \\ \mathbf{q}^T \tilde{M}_M \mathbf{q} - \beta_2 &> 0, \end{aligned} \tag{43}$$

where β_2 is defined as $\lambda_{\min}(M_M) + \beta_2 > 0$ such that $\tilde{M}_M$ is a positive definite matrix. Now the potential function (39) assumes the form

$$V(\mathbf{q}) = \|\mathbf{q}_d - \mathbf{q}\|^2 \left[\left(\sum_{j=1}^{m} \sum_{i=1}^{n} -k_1 \log\left(\frac{\mathbf{q}^T \tilde{M}_i^j \mathbf{q} - \beta_1}{2}\right)\right) - k_2 \log\left(\frac{\mathbf{q}^T \tilde{M}_M \mathbf{q} - \beta_2}{2}\right)\right]. \tag{44}$$

The above expression for the potential function comprises linear combinations of logarithmic functions. Since the summation of strictly convex functions is strictly convex, it suffices to analyze one of the terms in more detail, say,

$$V(\mathbf{q}) = \|\mathbf{q}_d - \mathbf{q}\|^2 \left[\sum_i -k \log\left(\frac{\mathbf{q}^T \tilde{M}_i^j \mathbf{q} - \beta_1}{2}\right)\right], \tag{45}$$

for some indices i and j. In this direction, the gradient of V is calculated as

$$\nabla V = \left(\frac{\partial}{\partial \mathbf{q}} \|\mathbf{q}_d - \mathbf{q}\|^2\right) \left[\sum_i -k \log\left(\frac{\mathbf{q}^T \tilde{M}_i^j \mathbf{q} - \beta_1}{2}\right)\right] + \|\mathbf{q}_d - \mathbf{q}\|^2 \left[\sum_i \frac{-2k}{\mathbf{q}^T \tilde{M}_i^j \mathbf{q} - \beta_1} \mathbf{q}^T \tilde{M}_i^j \right], \tag{46}$$

and the Hessian $\nabla^2 V$ is given as

$$\begin{aligned} \nabla^2 V = &\left(\frac{\partial^2}{\partial \mathbf{q}^2} \|\mathbf{q}_d - \mathbf{q}\|^2\right) \left[\sum_i \left(-k \log\left(\frac{\mathbf{q}^T \tilde{M}_i^j \mathbf{q} - \beta_1}{2}\right)\right)\right] \\ &+ \left(\frac{\partial}{\partial \mathbf{q}} \|\mathbf{q}_d - \mathbf{q}\|^2\right)^T \left[\sum_i \frac{-2k}{\mathbf{q}^T \tilde{M}_i^j \mathbf{q} - \beta_1} \mathbf{q}^T \tilde{M}_i^j \right] \\ &+ \left[\sum_i \frac{-2k}{\mathbf{q}^T \tilde{M}_i^j \mathbf{q} - \beta_1} \mathbf{q}^T \tilde{M}_i^j \right]^T \left(\frac{\partial}{\partial \mathbf{q}} \|\mathbf{q}_d - \mathbf{q}\|^2\right) \\ &+ \|\mathbf{q}_d - \mathbf{q}\|^2 \left[\sum_i \frac{4k}{(\mathbf{q}^T \tilde{M}_i^j \mathbf{q} - \beta_1)^2} (\mathbf{q}^T \tilde{M}_i^j)^T \mathbf{q}^T \tilde{M}_i^j \right] \\ &+ \|\mathbf{q}_d - \mathbf{q}\|^2 \left[\sum_i \frac{-2k}{\mathbf{q}^T \tilde{M}_i^j \mathbf{q} - \beta_1} \tilde{M}_i^j \right]. \end{aligned} \tag{47}$$

From the equation

$$\frac{\partial}{\partial \mathbf{q}} (\|\mathbf{q}_d - \mathbf{q}\|^2) = -2\mathbf{q}_d^T, \tag{48}$$

it follows that $\frac{\partial^2}{\partial \mathbf{q}^2} (\|\mathbf{q}_d - \mathbf{q}\|^2) = \mathbf{0}_{4\times 4}$ and $\|\mathbf{q}_d - \mathbf{q}\|^2 = 2 - 2\mathbf{q}_d^T \mathbf{q}$; thus, (47) simplifies to

$$\begin{aligned} \nabla^2 V = \sum_i \Bigg\{ &\frac{4k}{\mathbf{q}^T \tilde{M}_i^j \mathbf{q} - \beta_1} (\mathbf{q}_d \mathbf{q}^T \tilde{M}_i^j + \tilde{M}_i^j \mathbf{q} \mathbf{q}_d^T) \\ &+ (2 - 2\mathbf{q}_d^T \mathbf{q}) \frac{4k}{(\mathbf{q}^T \tilde{M}_i^j \mathbf{q} - \beta_1)^2} (\mathbf{q}^T \tilde{M}_i^j)^T \mathbf{q}^T \tilde{M}_i^j \\ &- (2 - 2\mathbf{q}_d^T \mathbf{q}) \frac{2k}{\mathbf{q}^T \tilde{M}_i^j \mathbf{q} - \beta_1} \tilde{M}_i^j \Bigg\}. \end{aligned} \tag{49}$$

Multiplying the last identity by $\mathbf{q}^T$ and $\mathbf{q}$ from the left and the right, respectively, yields

$$\begin{aligned} \mathbf{q}^T \nabla^2 V \mathbf{q} = \sum_i \Bigg\{ &\frac{8k}{\mathbf{q}^T \tilde{M}_i^j \mathbf{q} - \beta_1} \mathbf{q}^T \mathbf{q}_d (\mathbf{q}^T \tilde{M}_i^j \mathbf{q}) \\ &+ (2 - 2\mathbf{q}_d^T \mathbf{q}) \frac{4k}{(\mathbf{q}^T \tilde{M}_i^j \mathbf{q} - \beta_1)^2} (\mathbf{q}^T \tilde{M}_i^j \mathbf{q})^2 \\ &- \frac{2k(2 - 2\mathbf{q}_d^T \mathbf{q})}{\mathbf{q}^T \tilde{M}_i^j \mathbf{q} - \beta_1} (\mathbf{q}^T \tilde{M}_i^j \mathbf{q}) \Bigg\}. \end{aligned} \tag{50}$$

By letting

$$\gamma = \frac{4k \mathbf{q}^T \tilde{M}_i^j \mathbf{q}}{(\mathbf{q}^T \tilde{M}_i^j \mathbf{q} - \beta_1)^2}, \tag{51}$$

which is always a positive value, we obtain

$$\begin{aligned} \mathbf{q}^T \nabla^2 V \mathbf{q} = \sum_i \gamma \{ &(\mathbf{q}^T \tilde{M}_i^j \mathbf{q} - 3\beta_1) \mathbf{q}_d^T \mathbf{q} \\ &+ (\mathbf{q}^T \tilde{M}_i^j \mathbf{q} + \beta_1) \}, \end{aligned} \tag{52}$$

where $\beta_1 > 0$, and $\mathbf{q}^T \tilde{M}_i^j \mathbf{q} + \beta_1 > 0$ for all $\mathbf{q} \in \mathbf{Q}_P$ from (42). The above equation is a linear function of $\mathbf{q}_d^T \mathbf{q}$. Since $\mathbf{q}_d^T \mathbf{q} \in [-1,\ 1]$, one has

$$-\mathbf{q}^T \tilde{M}_i^j \mathbf{q} - \beta_1 < \mathbf{q}^T \tilde{M}_i^j \mathbf{q} - 3\beta_1 < \mathbf{q}^T \tilde{M}_i^j \mathbf{q} + \beta_1. \tag{53}$$

Note that the left-hand side of the inequality is derived from (42). Then, the right-hand side of the equality in (52)

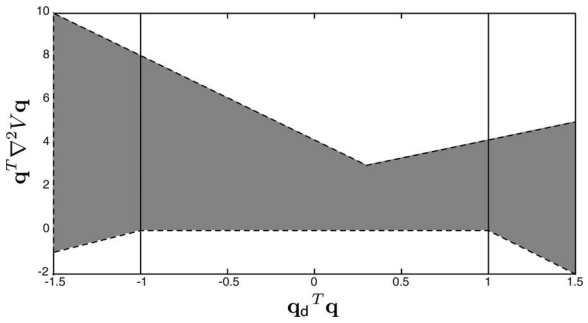

Fig. 5. Plot of $\mathbf{q}^T\nabla^2 V\mathbf{q}$ over $\mathbf{q}_d^T\mathbf{q}$ for $k = 0.005$.

remains positive for all $\mathbf{q}$, $\mathbf{q}_d \in \mathbf{Q}_P$. Therefore, the Hessian of V is positive definite, and V is smooth and strictly convex.

Fig. 5 depicts the plot of $\mathbf{q}^T\nabla^2 V\mathbf{q}$ over values of $\mathbf{q}_d^T\mathbf{q}$; Note that as long as $\mathbf{q}_d^T\mathbf{q} \in [-1,\ 1]$, $\mathbf{q}^T\nabla^2 V\mathbf{q}$ remains positive when $\mathbf{q} \neq \mathbf{q}_d$.

VI. FEEDBACK CONTROL LAW

In this section, we derive two control laws based on the logarithmic barrier potential function—now used as a Lyapunov function—for the purpose of showing almost global asymptotic stability of the corresponding closed loop system.

A. Model-Independent Control Law via a Direct Lyapunov Approach

Given the unit quaternion parameterization of the spacecraft attitude, a number of model-independent feedback control laws for the rigid body reorientation may be derived using the following procedure. In fact, a qualified strictly convex penalty (cost) function $V(\mathbf{q}) \geq 0$ and the linearity of quaternion kinematics (i.e., $\dot{\mathbf{q}} = \frac{1}{2}\mathbf{q} \otimes \tilde{\boldsymbol{\omega}}$) enable us to derive an almost globally stable control law on the quaternion domain. In this venue, given a cost function $V_{(\mathbf{q})}$ in unit quaternions, define

$$V_t = V + \frac{1}{2}\boldsymbol{\omega}^T J\boldsymbol{\omega}. \tag{54}$$

Then $V_t \geq 0$ for all $(\mathbf{q}, \boldsymbol{\omega})$, and the time derivative of V_t along (17, 18) is given by

$$\dot{V}_t = \nabla V^T(\frac{1}{2}\mathbf{q} \otimes \tilde{\boldsymbol{\omega}}) + \boldsymbol{\omega}^T J\dot{\boldsymbol{\omega}} \tag{55}$$

$$= \boldsymbol{\omega}^T \mathrm{Vec}[-\nabla V^* \otimes \frac{1}{2}\mathbf{q}] + \boldsymbol{\omega}^T \boldsymbol{u} \tag{56}$$

$$= \boldsymbol{\omega}^T(\mathrm{Vec}[-\nabla V^* \otimes \frac{1}{2}\mathbf{q}] + \boldsymbol{u}), \tag{57}$$

where the operator $\mathrm{Vec}[\cdot]$ denotes the vector part of $[\cdot]$. By taking

$$\boldsymbol{u} = -\alpha\omega + \frac{1}{2}\mathrm{Vec}[\nabla V^* \otimes \mathbf{q}], \tag{58}$$

where α denotes a positive parameter, (57) yields

$$\dot{V}_t = -\alpha\boldsymbol{\omega}^T\boldsymbol{\omega} \leq 0; \tag{59}$$

the implication of such an observation is now formally discussed.

PROPOSITION 7 The feedback control law given by (58) leads the cost function V, as well as the combined cost function V_t, to converge to zero asymptotically.

PROOF Consider V_t as a candidate Lyapunov function. Let $S = \{\boldsymbol{\omega} | \dot{V}_t = 0\}$. From (59), it follows that $\dot{V}_t = 0$ implies that $\boldsymbol{\omega} = 0$, and in turn $\boldsymbol{u} = 0$ by (18). Similarly, $\boldsymbol{\omega} = 0$ and $\boldsymbol{u} = 0$ implies that $\nabla V^* = 0$ in (58) since $\mathbf{q} \neq \mathbf{0}$. Additionally, the fact that V is strictly convex leads to the equivalency

$$\{\mathbf{q} | \nabla V(\mathbf{q}) = \nabla V^*(\mathbf{q}) = \mathbf{0}\} \Leftrightarrow \{\mathbf{q} | V(\mathbf{q}) = 0\}; \tag{60}$$

hence, the invariant set contains $\mathbf{q}_d$ for which we have $V(\mathbf{q}_q) = 0$; that is,

$$\{\boldsymbol{\omega} | \dot{V}_t = 0\} \Rightarrow \{(\boldsymbol{\omega}, \mathbf{q}) | V(\mathbf{q}) = 0 \text{ and } \boldsymbol{\omega} = 0\}. \tag{61}$$

Therefore, by LaSalle's invariance principle [39], the equilibrium $([\mathbf{q}_d, \boldsymbol{\omega})$ is asymptotically stable.

REMARK 1 It has been shown that a unit quaternion-based continuous feedback control almost globally asymptotically stabilizes the system. This terminology originates because the dynamics also admits an unstable equilibrium point $(-\mathbf{q}_d, \boldsymbol{\omega})$; for more detailed discussions on this point, see [40–42].

Now, we propose a cost function for the attitude reorientation in the presence of attitude-constrained zones. From (39), we have

$$V_t = V(\mathbf{q}) + \frac{1}{2}\boldsymbol{\omega}^T J\boldsymbol{\omega}, \tag{62}$$

where $\mathbf{Q}_P \subseteq \mathbf{U}_\mathbf{q}$. Because $V(\mathbf{q})$ is strictly convex in $\mathbf{q}$, according to Proposition 8, the dynamics induced by the negative gradient of V_t guides the state $\mathbf{q}$ toward the final $\mathbf{q}_d$ as V_t converges to zero. Moreover, if $\mathbf{q} \to \partial\mathbf{Q}_P$ or $\boldsymbol{\omega} \to \infty$, or one has $V_t \to \infty$, which violates the (negative) gradient flow property of the underlying dynamics, from (58), we thus obtain an almost globally stabilizing model-independent control

$$\boldsymbol{u} = -\alpha\omega - \mathrm{Vec}[(l_g\mathbf{q}_d^* - \frac{1}{2}\|\mathbf{q}_d - \mathbf{q}\|^2\nabla l_g^*) \otimes \mathbf{q}], \tag{63}$$

where $\alpha > 0$, and l_g denotes the summation of the logarithmic barrier potentials in (39) as

$$l_g = -\sum_{j=1}^{m}\sum_{i=1}^{n} k_1 \log\left(\frac{\mathbf{q}^T M_i^j \mathbf{q}}{2}\right) - k_2 \log\left(\frac{\mathbf{q}^T M_M \mathbf{q}}{2}\right). \tag{64}$$

B. Model-Dependent Control Law via Modified Backstepping

Our second type of feedback control for an attitude-constrained maneuver is obtained using the modified backstepping method. This is achieved by

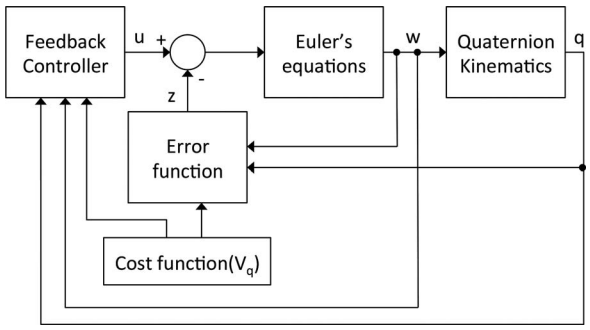

Fig. 6. Modified backstepping controller scheme.

observing that the spacecraft dynamics described by (17) and (18) have a "cascaded" structure, thus making these dynamics suitable for control design based on the backstepping method [43]. However, one of the drawbacks of the conventional backstepping method is typically excessive control during the initial phase of the trajectory and sluggish closed-loop dynamics in the later part of the trajectory—both of which are undesirable in practice. In this direction, we adopt the modified backstepping method, as discussed in [8], and propose an improved nonlinear error function for the constrained attitude control problem.

Let us first note that by letting

$$\dot{\mathbf{q}}(t) = -\nabla V(\mathbf{q}), \tag{65}$$

we have

$$\dot{V} = \frac{\partial V}{\partial \mathbf{q}} \cdot \frac{\partial \mathbf{q}}{\partial t} = \nabla V^T \cdot \dot{\mathbf{q}} = -\|\nabla V\|^2 < 0, \tag{66}$$

for all $\mathbf{q} \neq \mathbf{q}_d$, qualifying V as a strong Lyapunov function for the dynamics described by (17) and (18), with respect to the equilibrium $\mathbf{q}_d$. Note that ∇V has units of $1/s$ because parameters k_1 and k_2 have units of $1/s$ in (39). Our strategy involves considering $\tilde{\boldsymbol{\omega}}$ in (17) as a "virtual" control input in order to have an asymptotically stable system in (17) after closing the loop. Using quaternion identities, we now set

$$\tilde{\boldsymbol{\omega}}_c = -2\mathbf{q}^\star \otimes \nabla V. \tag{67}$$

Note that $\tilde{\boldsymbol{\omega}}_c$ has the form of quaternion with the last element identically zero as $\tilde{\boldsymbol{\omega}}_c = [\omega_c^T \ 0]^T$. Let $\tilde{\mathbf{z}}$ denote the error between $\tilde{\boldsymbol{\omega}}$ and its desired value $\tilde{\boldsymbol{\omega}}_c$ as,

$$\tilde{z} = \tilde{\boldsymbol{\omega}} - \tilde{\boldsymbol{\omega}}_c = \tilde{\boldsymbol{\omega}} + 2\mathbf{q}^\star \otimes \nabla V, \tag{68}$$

where $\tilde{\mathbf{z}} = [z^T \ 0]^T$. In the control scheme depicted in Fig. 6, the error function $\tilde{z}$ acts as a feed-forward term and causes excessive control inputs in the initial phase of the control input when the error is large. Hence, we propose a modified error function as

$$\tilde{\mathbf{z}} = \alpha \arctan \beta(\tilde{\boldsymbol{\omega}} - \tilde{\boldsymbol{\omega}}_c) = \alpha \arctan \beta(\tilde{\boldsymbol{\omega}} + 2\mathbf{q}^\star \otimes \nabla V), \tag{69}$$

where α and β are the shaping parameters [8]. Thereby,

$$\tilde{\boldsymbol{\omega}} = \frac{1}{\beta} \tan\left(\frac{1}{\alpha}\tilde{\mathbf{z}}\right) - 2\mathbf{q}^\star \otimes \nabla V. \tag{70}$$

Next, by plugging the above expression for $\tilde{\boldsymbol{\omega}}$ in (17), we obtain

$$\begin{aligned}\dot{\mathbf{q}} &= \frac{1}{2}\mathbf{q} \otimes \tilde{\boldsymbol{\omega}} \\ &= \frac{1}{2}\mathbf{q} \otimes \left(\frac{1}{\beta}\tan\left(\frac{1}{\alpha}\tilde{\mathbf{z}}\right)\right) - \nabla V.\end{aligned} \tag{71}$$

Additionally, the time derivative of the vector part of (69) along with (18) is now given as

$$\begin{aligned}J\dot{\mathbf{z}} &= J\frac{d}{dt}\alpha \arctan \beta(\boldsymbol{\omega} - \boldsymbol{\omega}_c) \\ &= C_1(R(\boldsymbol{\omega})J\boldsymbol{\omega}(t) + \boldsymbol{u}(t) - J\dot{\boldsymbol{\omega}}_c),\end{aligned} \tag{72}$$

where $C_1 = \alpha\beta\left[I_3 + \beta^2 \text{Diag}(\boldsymbol{\omega} - \boldsymbol{\omega}_c)^2\right]^{-1}$.

To find the input $\boldsymbol{u}(t)$ that stabilizes the system Equations (71) and (72), we define an augmented candidate Lyapunov function

$$V(\mathbf{q}, z) = V + \frac{1}{2}z^T J z. \tag{73}$$

Taking the time derivative of V along the trajectories of (71), (72), we obtain

$$\begin{aligned}\dot{V} &= \nabla V^T \dot{\mathbf{q}} + z^T J\dot{\mathbf{z}} \\ &= \nabla V^T(\frac{1}{2}\mathbf{q} \otimes \tilde{\mathbf{z}}) - \|\nabla V\|^2 + z^T C_1(R(\boldsymbol{\omega})J\boldsymbol{\omega}(t) \\ &\quad + \boldsymbol{u}(t) - J\dot{\boldsymbol{\omega}}_c).\end{aligned} \tag{74}$$

By rearranging the term $\nabla V^T(\frac{1}{2}\mathbf{q} \otimes \tilde{\mathbf{z}})$ and using quaternion identities, (74) now assumes the form

$$\begin{aligned}\dot{V} &= \nabla V^T(\frac{1}{2}\mathbf{q} \otimes \tilde{\mathbf{z}}) - \|\nabla V\|^2 + z^T C_1(R(\omega)J\boldsymbol{\omega}(t) \\ &\quad + \boldsymbol{u}(t) - J\dot{\boldsymbol{\omega}}_c) \\ &= z^T(\frac{1}{2}q_0 \text{Vec}[\nabla V_q] + \frac{1}{2}\text{Vec}[\nabla V] \times \mathbf{q} - \frac{1}{2}\nabla V_0 \mathbf{q}) \\ &\quad - \|\nabla V\|^2 z^T C_1(R(\boldsymbol{\omega})J\boldsymbol{\omega}(t) + \boldsymbol{u}(t) - J\dot{\boldsymbol{\omega}}_c) \\ &= z^T(\frac{1}{2}q_0 \text{Vec}[\nabla V] + \frac{1}{2}\text{Vec}[\nabla V] \times \boldsymbol{q} - \frac{1}{2}\nabla V_0 \boldsymbol{q} \\ &\quad + C_1[R(\omega)J\omega(t)u(t) - J\dot{\boldsymbol{\omega}}_c]) - \|\nabla V\|^2,\end{aligned} \tag{75}$$

where $\nabla V = [\text{Vec}[\nabla V]^T \nabla V_0]^T$. Therefore, by choosing the actuator torque as

$$\begin{aligned}u(t) = J\dot{\boldsymbol{\omega}}_c - R(\boldsymbol{\omega})J\boldsymbol{\omega}(t) - C_1^{-1}[\frac{1}{2}q_0 \text{Vec}[\nabla V] \\ -\frac{1}{2}\text{Vec}[\nabla V] \times \boldsymbol{q} + \frac{1}{2}\nabla V_0 \boldsymbol{q} - z],\end{aligned} \tag{76}$$

one has

$$\dot{V} = -\|\nabla V\|^2 - z^T z \leq 0, \tag{77}$$

guaranteeing that the overall system is asymptotically stable. From (69), on the other hand, we note that

$$z = \alpha \arctan \beta\left(\text{Vec}[\tilde{\boldsymbol{\omega}} + 2\mathbf{q}^\star \otimes \nabla V]\right). \tag{78}$$

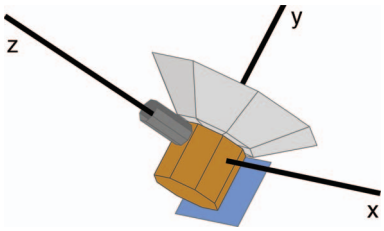

Fig. 7. Spacecraft configuration with one light-sensitive instrument (Z axis) and high-gain antenna (Y axis).

Now, rewriting the actuator torque $\boldsymbol{u}$ in $\boldsymbol{\omega}$ using the quaternion identities, we obtain,

$$\boldsymbol{u}(\boldsymbol{\omega}) = J\dot{\boldsymbol{\omega}}_c - R(\boldsymbol{\omega})J\omega + \frac{1}{2}C_2\mathrm{Vec}[\nabla V^\star \otimes \mathbf{q}] - z, \quad (79)$$

where

$$C_2 = (1/\alpha\beta)[I_3 + \beta^2\mathrm{Diag}(\boldsymbol{\omega} - \boldsymbol{\omega}_c)^2].$$

The next step pertains to computing the term $\dot{\omega}_c$, which appears in the control law (79). This term is the time derivative of (67), which should be computed directly when the control law is implemented. In the meantime, the time derivative of the vector part of $\tilde{\boldsymbol{\omega}}_c$ can be given as,

$$\begin{aligned}\dot{\boldsymbol{\omega}}_c &= \frac{\partial}{\partial t}(2\nabla V_0\boldsymbol{q} - 2q_0\mathrm{Vec}[\nabla V] + 2\boldsymbol{q} \times \mathrm{Vec}[\nabla V]) \\ &= -2(\mathrm{Vec}[\dot{\mathbf{q}}^\star \otimes \nabla \boldsymbol{V} + \mathbf{q}^\star \otimes \nabla^2 V\dot{\mathbf{q}}]). \end{aligned} \quad (80)$$

VII. SIMULATION RESULTS

In this section, to illustrate the effectiveness of the proposed methodology to constrained motion planning, we present simulation results for three distinct scenarios. In all of these cases, it has been assumed that the spacecraft carries a light-sensitive instrument with a fixed boresight in the spacecraft body axes, directed along the Z direction. Moreover, it is assumed that a high-gain antenna has been mounted on the spacecraft such that its boresight is directed along the Y axis (see Fig. 7). We note that the k_i parameters in (39) influence the convergence rate of the algorithm since the corresponding logarithmic terms rapidly increase as the norm $\|\mathbf{q}_d - \mathbf{q}\|^2$, associated with an attraction term toward the destination attitude, decreases. From the simulations presented here, the k_i values are chosen around 0.005 for each constraint, while the spacecraft's moment of inertia is set as

$$J = \mathrm{Diag}[694,\ 572,\ 360]\ \mathrm{kg}\cdot\mathrm{m}^2. \quad (81)$$

Generally, larger values of k_i prolong convergence to the destination attitude, particularly when the desired attitude is close to the boundary of the constraint set.

A. Case 1 (Four Attitude-Forbidden Zones)

We consider the case in which the spacecraft is retargeting its telescope while avoiding four attitude-forbidden zones in the spacecraft rotational configuration space. Both initial and desired attitudes are randomly chosen in the attitude-permissible zone,

TABLE I
Case 1: Simulation Parameters (Four Attitude-Forbidden Zones)

	Constrained Object	Angle
(a) Initial attitude	[0.174, −0.934, −0.034]	40 deg
[−0.187 −0.735 −0.450 −0.470]	[0, 0.707 0.707]	40 deg
(a) Desired attitude	[−0.853, 0.436, −0.286]	30 deg
[0.592 −0.675 −0.215 0.382]	[−0.122, −0.140, −0.983]	20 deg
(b) Initial attitude	[0.163, −0.986, 0.02]	20 deg
[0.452 0.682 0.465 −0.336]	[0, 0.573, 0.819]	30 deg
(b) Desired attitude	[−0.067, −0.462, −0.88]	20 deg
[0.029 0.659 −0.619 −0.425]	[−0.813, 0.548, −0.19]	40 deg

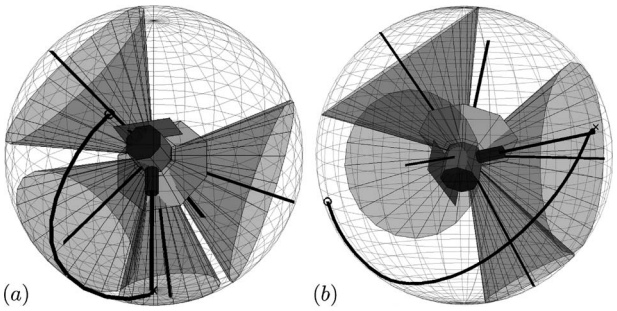

Fig. 8. Case 1: Trace of telescope pointing direction on celestial sphere generated by model-independent control law. On sphere, "circle′" and "cross′" indicate directions of initial and final orientations, respectively.

satisfying the following inequalities for all i,

$$\mathbf{q}_0^T M_i^1 \mathbf{q}_0 < 0 \quad \text{and} \quad \mathbf{q}_d^T M_i^1 \mathbf{q}_d < 0, \quad (82)$$

where $\mathbf{q}_0$ and $\mathbf{q}_d$ are the initial and desired unit quaternions, respectively. These attitude-forbidden zones are randomly chosen with the provision of not overlapping with each other in this example; however, this is not necessary in general as long as a feasible trajectory exists. Also, the identity unit quaternion $\mathbf{q}_\mathbf{I}$ is chosen to have the opposite sign as the scalar part of $\mathbf{q}_d^\star \otimes \mathbf{q}_0$ to promote avoiding the unwinding phenomenon. We conduct the simulations in the context of two different scenarios and two types of control laws discussed in this paper. In Table I, the initial and desired spacecraft attitudes are given in unit quaternions as well as the normalized position vectors, indicating four constrained sets (forbidden zones), all expressed with respect to the inertial frame. The potential function for this case is given as

$$V(\mathbf{q}) = \|\mathbf{q}_d - \mathbf{q}\|^2 \left[\left(\sum_{i=1}^{4} -k_1 \log\left(-\frac{\boldsymbol{q}^T M_i^1 \boldsymbol{q}}{2}\right)\right)\right], \quad (83)$$

where M_i^1 depends on the ith position vector indicating the corresponding constraint set. Fig. 8 represents the trajectories of the direction in which the light-sensitive instrument points on the celestial sphere generated by model-independent control laws with the initial attitude (denoted by k_i) and the desired attitude (denoted by $\times$). In Fig. 9 the same trajectories are depicted on the cylindrical projection of the corresponding celestial spheres for model-independent and model-dependent control laws. For comparison, Fig. 9 also traces the analogous plots for

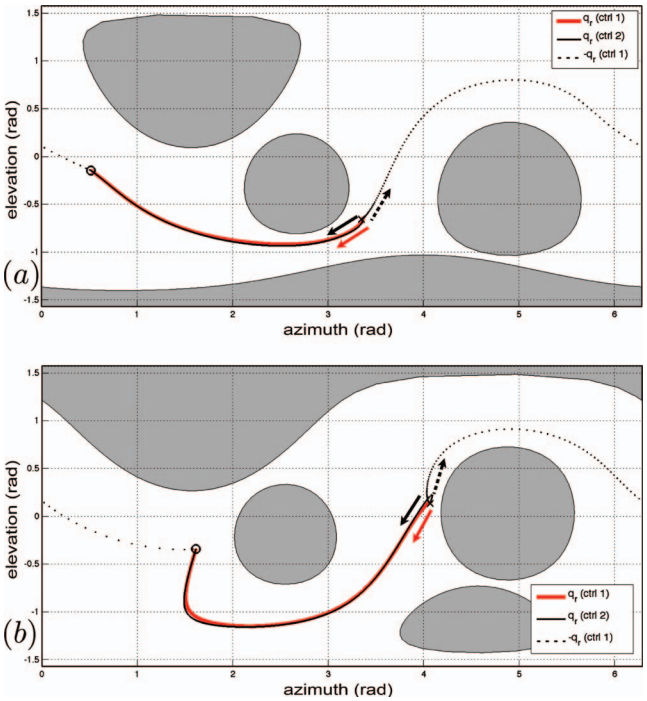

Fig. 9. Case 1: Reorientation trajectories in two-dimensional (2D) cylindrical projection for two types of controls (solid line); for comparison, nongeodesic trajectories are also depicted (dotted line).

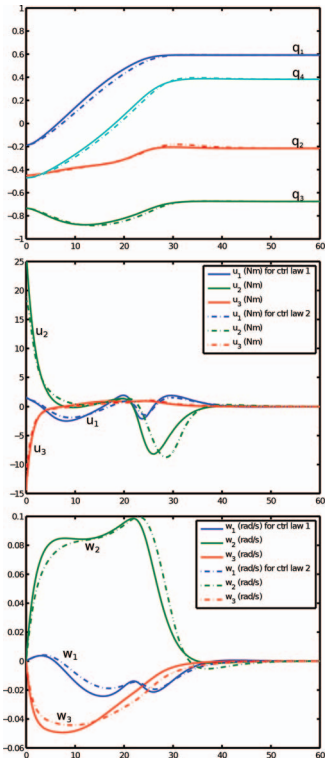

Fig. 10. Case 1-a: Time histories for quaternion trajectories, control inputs, and angular velocities; time axis is in seconds.

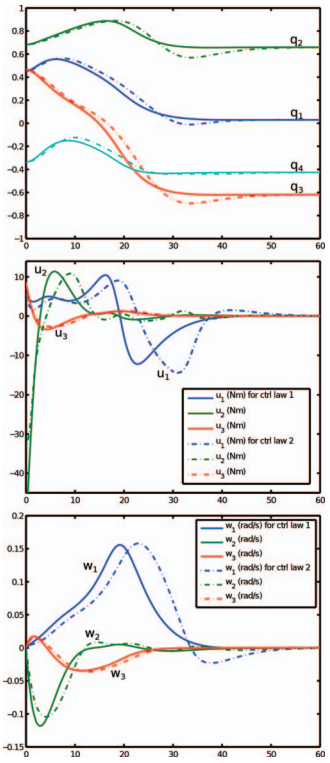

Fig. 11. Case 1-b: Time histories for quaternion trajectories, control inputs, and angular velocities; time axis is in seconds.

the nongeodesic (longer) trajectories obtained using $-\mathbf{q}_\mathbf{I}$. As shown in Figs. 10 and 11, the required final states are achieved asymptotically in all scenarios.

B. Case 2 (One Attitude-Mandatory Zone)

The purpose of this simulation scenario is to verify the utility of the proposed methodology for reorientation maneuvers frequently required for microsatellite formation flying. Because each microsatellite is not fully equipped with the necessary inertial position sensors on-board (e.g., star trackers), it becomes important that the on-board guidance system has the ability to point the directional antenna in a specified direction for interspacecraft communication and sensing. Therefore in this simulation, we have considered a reorientation maneuver within the attitude-mandatory zone associated with an on-board antenna. In these simulations, the moment of inertia and the shaping parameter k_2 are set as

$$J = \text{Diag}(2.4,\ 3.1,\ 1.4)\ \text{kg}\cdot\text{m}^2 \quad \text{and} \quad k_2 = 0.02. \tag{84}$$

The logarithmic barrier potential function for this case assumes the form

$$V(\mathbf{q}) = \|\mathbf{q_d} - \mathbf{q}\|^2 \left[-k_2 \log\left(\frac{\mathbf{q}^T M_M \mathbf{q}}{2}\right)\right], \tag{85}$$

where M_M is given in (26). The initial and desired attitudes, on the other hand, which should be in the mandatory zone, have been specified as

$$\mathbf{q}_0^T M_M \mathbf{q}_0 > 0 \quad \text{and} \quad \mathbf{q}_\mathbf{d}^T M_M \mathbf{q}_\mathbf{d} > 0, \tag{86}$$

where $\mathbf{q}_0$, $\mathbf{q}_d$ are the initial and desired spacecraft attitudes, respectively. Figs. 12 and 13 depict, respectively, the model-dependent and model-independent control generated reorientation trajectory on the celestial sphere,

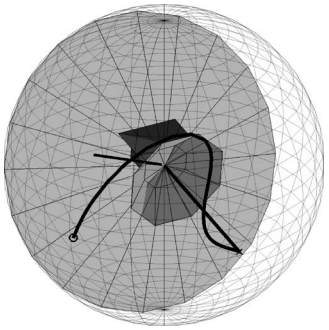

Fig. 12. Case 2: Model-dependent control-generated trajectory in celestial attitude-mandatory zone.

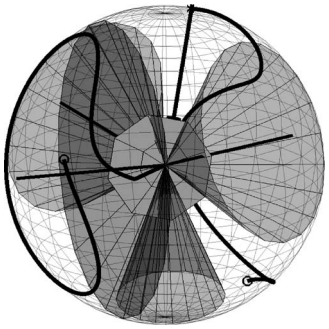

Fig. 13. Case 3: Model-independent control-generated trajectory in the celestial attitude-mandatory and -forbidden zones.

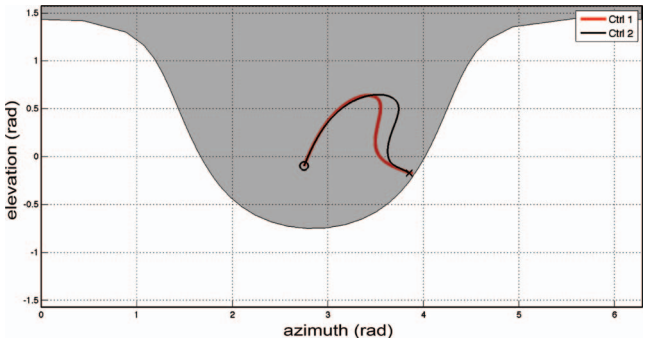

Fig. 14. Case 2: Reorientation trajectories in 2D cylindrical projection space in presence of one attitude-mandatory zone.

and Fig. 14 represents the trajectories governed by two types of control laws; see Fig. 16 for the corresponding simulation results as well as Table II for the simulation parameters. In this simulation scenario, we have assumed that the spacecraft is initially stationary.

REMARK 2 It is worth noting that in the presence of an attitude-mandatory zone, it becomes more important to choose the right unit quaternion for the geodesic (shorter) trajectories. Otherwise, the nongeodesic rotation will lead it to the boundary of the constrained set and potentially cause a large number of oscillations.

C. Case 3 (Three Attitude-Forbidden Zones and One Mandatory Zone)

In case 3, we examine a more complex reorientation maneuver (see Fig. 18) for keeping a fixed boresight

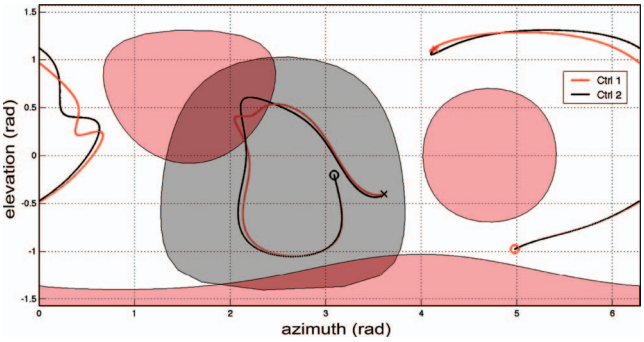

Fig. 15. Case 3: Reorientation trajectories in 2D cylindrical projection space. Shown trajectory is geodesic. Nongeodesic rotation (from injudiciously signed $\mathbf{q}$) will cause many oscillations around boundary.

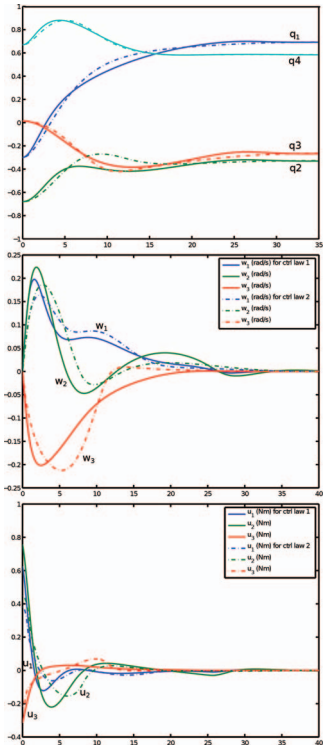

Fig. 16. Case 2: Time histories for quaternion trajectories, control inputs, and angular velocities; time axis is in seconds.

TABLE II
Case 2 Constraint Parameters

	Constrained Object	Angle	Type
Initial attitude [−0.299 −0.679 0.014 0.669]	[−0.852 0.265 0.449]	70 deg	M
Desired attitude [0.693 –0.327 −0.263 0.585]			

vector (e.g., an antenna) within a certain angle to communicate continuously with the ground station while the spacecraft is retargeting its light-sensitive instrument to avoid multiple bright objects or constrained zones. In this case, the feasible spacecraft attitude for reorientation can be represented using a combination of an attitude-mandatory zone and attitude-forbidden zones. For this scenario, the antenna has been aligned along the Z axis

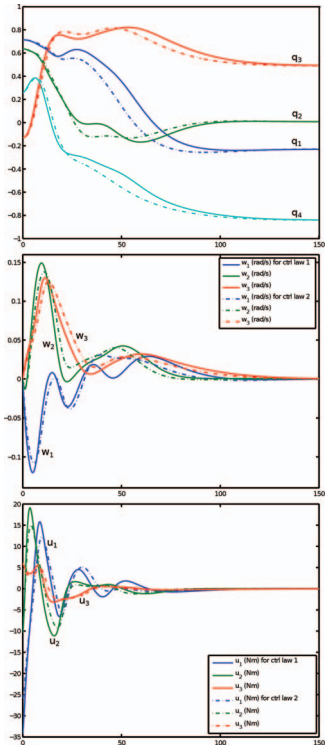

Fig. 17. Case 3: Time histories for quaternion trajectories, control inputs, and angular velocities; time axis is in seconds.

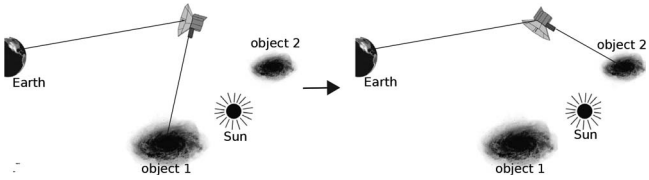

Fig. 18. Reorientation under a combination of attitude-mandatory and -forbidden zones (case 3).

while the sensitive instrument has been aligned along the Y axis (see Fig. 7). This case is distinct from the earlier ones, in that for the spacecraft reorientation to be feasible, one has to take an additional condition into account along with

$$\mathbf{q}_0^T M_M(\theta_M)\mathbf{q}_0 > 0 \text{ and } \mathbf{q}_0^T M_i^j \mathbf{q}_0 < 0, \text{ for all } i, j, \quad (87)$$

and

$$\mathbf{q}_d^T M_M(\theta_M)\mathbf{q}_d^T > 0 \text{ and } \mathbf{q}_d^T M_i^j \mathbf{q}_d^T < 0, \text{ for all } i, j. \quad (88)$$

REMARK 3 We note that since this case includes an attitude-mandatory zone as well as attitude-forbidden zones, selecting the right signed unit quaternion for geodesic rotation is more important than in the other cases. Depending on the initial configuration, the nongeodesic rotation may result in a large number of oscillations to reach the desired orientation.

In this direction, let us adopt the potential function,

$$V(\mathbf{q}) = \|\mathbf{q_d} - \mathbf{q}\|^2 \left[\left(\sum_{i=1}^{3} -k_1 \log\left(-\frac{\mathbf{q}^T M_i^1 \mathbf{q}}{2} \right) \right) \right.$$

TABLE III
Simulation Settings for Case 3

	Constrained Object	Angle	Type
Initial attitude	[−0.813 0.548 −0.192]	70 deg	M
[0.714 0.637−0.13 0.26]	[0 −1 0]	40 deg	F
Desired attitude	[0 0.819 0.573]	40 deg	F
[−0.23 0.008 0.491 −0.84]	[−0.122 −0.139 −0.982]	20 deg	F

$$\left. -k_2 \log\left(\frac{\mathbf{q}^T M_M \mathbf{q}}{2} \right) \right], \quad (89)$$

where M_1, M_2, and, M_3 are associated with the three attitude-forbidden zones, and M_M corresponds to the attitude-mandatory zone. We use the spacecraft's moments of inertia as in (81). Fig. 15 demonstrate a reorientation maneuver while keeping the antenna's boresight vector within 70 degrees of the permissible cone by the proposed control laws. The simulation parameters for this scenario are given in Table III. Fig. 17 shows the time histories for the quaternion trajectories and control inputs along the three independent spacecraft axes, as well as the time history for the spacecraft angular velocity.

VIII. CONCLUSIONS AND FUTURE WORK

In this paper, an autonomous maneuver-planning algorithm for three-axis attitude reorientation in the presence of multiple types of attitude-constrained zones has been proposed. This has been achieved via a convex logarithmic barrier potential that is built on the convex parameterization of attitude constraint sets in the unit quaternion space. Based on such a potential function, we then proceeded to develop two types of control laws, referred to as model independent and model dependent, for the constrained attitude control problem. Simulation results have then been presented for three distinct scenarios.

The main advantage of the proposed algorithms are their feedback form and almost global convergence properties from any initial condition, as well as their tractability and scalability for distinct classes of attitude-constrained zones. Since our approach is analytical and computationally tractable, it is suitable for on-board autonomous spacecraft attitude maneuver planning.

ACKNOWLEDGMENT

The authors gratefully acknowledge the suggestions of the reviewers and the Associate Editor in revising the original version of the paper.

REFERENCES

[1] Koenig, J. D.
A novel attitude guidance algorithm for exclusion zone avoidance.
In *Proceedings of the IEEE 2009 Aerospace Conference*, **14**, Big Sky, MT, Mar. 2009, 1–10.

[2] Mortensen, R. E.
A globally stable linear attitude regulator.
International Journal of Control, **8**, 3 (1968), 297–302.

[3] Bach, R., and Paielli, R.
Linearization of attitude control error dynamics.
IEEE Transactions on Automatic Control, **38**, 10 (1993), 1521–1525.

[4] Tsiotras, P., Corless, M., and Longuski, J. M.
A novel approach to the attitude control of axisymmetric spacecraft.
Automatica, **31**, 8 (1995), 1099–1112.

[5] Gennaro, S. D.
Output stabilization of flexible spacecraft with active vibration suppression.
IEEE Transactions on Aerospace and Electronic Systems, **39**, 3 (2003), 747–759.

[6] Singla, P., Subbarao, K., and Junkins, J.
Adaptive output feedback control for spacecraft rendezvous and docking under measurement uncertainty.
Journal of Guidance, Control and Dynamics, **29**, 4 (2006), 892–902.

[7] Jin, E. D., and Sun, Z. W.
Robust attitude tracking control of flexible spacecraft for achieving globally asymptotic stability.
International Journal of Robust and Nonlinear Control, **19**, 11 (2009), 1201–1223.

[8] Kim, K., and Kim, Y.
Robust backstepping control for slew maneuver using nonlinear tracking function.
IEEE Transactions on Control Systems Technology, **11**, 6 (2003), 822–829.

[9] Singh, S. N., and Yim, W.
Nonlinear adaptive backstepping design for spacecraft attitude control using solar radiation pressure.
In *Proceedings of the 41st IEEE Conference on Decision and Control*, Las Vegas, NV, Dec. 2002.

[10] Kristiansen, R., and Nicklasson, P. J.
Satellite attitude control by quaternion-based backstepping.
In *Proceedings of American Control Conference*, Portland, OR, Jan. 2005.

[11] Xin, M., and Pan, H.
Indirect robust control of spacecraft via optimal control solution.
IEEE Transactions on Aerospace and Electronic Systems, **48**, 2 (2012), 1798–1809.

[12] Horri, N. M., Palmer, P., and Roberts, M.
Gain-scheduled inverse optimal satellite attitude control.
IEEE Transactions on Aerospace and Electronic Systems, **48**, 3 (2012), 2437–2457.

[13] Haddad, W. M., Chellaboina, V. S., Fausz, J. L., and Leonessa, A.
Optimal nonlinear robust control for nonlinear uncertain cascade systems. *Proceedings of the American Control Conference*, **1**, Albuquerque, NM, 4–6 Jun 1997, 403–407.

[14] Wen, J. T., and Kreutz-Delgado, K.
The attitude control problem.
IEEE Transactions on Automatic Control, **36**, 10 (1991), 1148–1162.

[15] Wie, B., and Barba, P. M.
Quaternion feedback for spacecraft large angle maneuvers.
Journal of Guidance, Control and Dynamics, **8**, 3 (1985), 360–365.

[16] Mayhew, C. G., Sanfelice, R. G., and Teel, A. R.
Quaternion-based bybrid control for robust global attitude tracking.
IEEE Transactions on Automatic Control, **56**, 11 (Nov. 2011), 2555–2566.

[17] Joshi, S. M., Kelkar, A. G., and Wen, J. T.
Robust attitude stabilization of spacecraft using nonlinear quaternion feedback.
IEEE Transactions on Automatic Control, **40**, 10 (1995), 1800–1803.

[18] McInnes, C. R.
Large angle slew maneuvers with autonomous sun vector avoidance.
AIAA Journal of Guidance, Control and Dynamics, **17**, 4 (1994), 875–877.

[19] McInnes, C. R.
Nonlinear control for large angle attitude slew maneuvers.
In *Proceedings of the Third ESA Symposium on Spacecraft Guidance, Navigation, and Control*, 543–548, 1996.

[20] McInnes, C. R.
Potential function methods for autonomous spacecraft guidance and control.
In *Proceedings of the AAS/AIAA Astrodynamics Specialist Conference*, San Diego, CA, **90**, 29–31 July 1996, 2093–2109.

[21] Spindler, K.
New methods in on-board attitude control.
Advanced in the Astronautical Sciences, **100**, 2 (1998), 111–124.

[22] Hablani, H. B.
Attitude commands avoiding bright objects and maintaining communication with ground station.
Journal of Guidance, Control, and Dynamics, **22**, 6 (1999), 759–767.

[23] Frakes, J. P., Henretty, D. A., Flatley, T. W., Markley, F. L., San, J., and Lightsey, E. G.
SAMPEX science pointing with velocity avoidance.
In *Proceedings of the AAS/AIAA Spaceflight Mechanics Meeting*, Colorado Springs, CO, 24–26 Feb. 1992, 949–966.

[24] Frazzoli, E., Dahleh, M. A., Feron, E., and Kornfeld, R. P.
A randomized attitude slew planning algorithm for autonomous spacecraft.
In *Proceedings of the AAIA Guidance, Navigation, and Control Conference*, Montreal, Quebec, Canada, 6–9 Aug. 2001.

[25] Kornfeld, R. P.
On-board autonomous attitude maneuver planning for planetary spacecraft using genetic algorithms.
In *Proceedings of the AIAA Conference on Guidance, Navigation and Control*, Austin, TX, 11–14 Aug. 2003.

[26] Cui, P., Zhong, W., and Cui, H.
Onboard spacecraft slew-planning by heuristic state-space search and optimization.
In *Proceedings of the International Conference on Mechatronics and Automation*, Harbin, China, 5–8 Aug. 2007, 2115–2119.

[27] Kjellberg, H. C., and Lightsey, E. G.
Discretized constrained attitude pathfinding and control for satellites.
Journal of Guidance, Control, and Dynamics, **36**, 5 (2013), 1301–1309.

[28] Kim, Y., Mesbahi, M., Singh, G., and Hadaegh, F.
On the convex parametrization of spacecraft orientation in the presence of constraints and its applications.
IEEE Transactions on Aerospace and Electronic Systems, **46**, 3 (2010), 1097–1109.

[29] Kim, Y., and Mesbahi, M.
Quadratically constrained attitude control via semidefinite programming.
IEEE Transactions on Automatic Control, **49**, 5 (2004), 731–735.

[30] Ahmed, A., Alexander, J., Boussalis, D., Breckenridge, W., Macala, G., Mesbahi, M., San Martin, M., Singh, G., and Wong, E.
Cassini control analysis book. Jet Propulsion Laboratory, California Institute of Technology, Pasadena, CA, Tech. Rep., 1998.

[31] Koditschek, D.E.
Application of a new Lyapunov function to global adaptive tracking.
In *Proceedings of the 27th Conference on Decision and Control*, Austin, TX, Dec. 1988, 63–68.

[32] Shuster, M. D.
A survey of attitude representations.
The Journal of the Astronautical Sciences, **41**, 4 (1993), 438–517.

[33] Bhat, S., and Bernstein, D. S.
A topological obstruction to continuous global stabilization of rotational motion and the unwinding phenomenon.
Systems & Control Letters, **39**, 1 (2000), 63–70.

[34] Mayhew, C. G., Sanfelice, R. G., and Teel, A. R.
On quaternion-based attitude control and the unwinding phenomenon.
In *Proceedings of the American Control Conference*, San Francisco, CA, 29 June–1 July 2011, 299–304.

[35] Mayhew, C. G., Sanfelice, R. G., and Teel, A. R.
On path-lifting mechanisms and unwinding in quaternion-based attitude control.
IEEE Transactions on Automatic Control, **58**, 5 (2013), 1179–1191.

[36] Han, D., Wei, Q., and Li, Z.
Kinematic control of free rigid bodies using dual quaternions.
International Journal of Automation and Computing, **5**, 3 (July 2008), 319–324.

[37] Wertz, J. R.
Spacecraft Attitude Determination and Control. Norwell, MA: Kluwer, 1978.

[38] Singh, G., Macala, G., Wong, E., and Rasmussen, R.
A constraint monitor algorithm for the Cassini spacecraft.
In *Proceedings of the AIAA Guidance, Navigation, and Control Conference*, New Orleans, LA, Aug. 1997, 272–282.

[39] Khalil, H. K.
Nonlinear Systems. Prentice Hall, 2002.

[40] Bharadwaj, S., Osipchuk, M., Mease, K. D., and Park, F. C.
Geometry and inverse optimality in global attitude stabilization.
Journal of Guidance, Control, and Dynamics, **21**, 6 (1998), 930–939.

[41] Song, Y. D., and Cai, W. C.
New intermediate quaternion based control of spacecraft: part I—almost global attitude tracking.
International Journal of Innovative Computing, Information and Control, **8**, 10B (Oct. 2012), 7307–7319.

[42] Sanyal, A., and Chaturvedi, N.
Almost global robust attitude tracking control of spacecraft in gravity.
In *Proceedings of the AIAA Conference on Guidance, Navigation and Control*, Honolulu, HI, Aug. 2008.

[43] Freeman, R. A., and Kokotović, P.
Robust Nonlinear Control Design: State Space and Lyapunov Techniques. Boston: Birkhäuser, 1996.

Unsik Lee obtained his B.S. degree in aerospace and mechanical engineering from Inha University, Korea, and M.S. and Ph.D. degrees in aeronautics and astronautics from the University of Washington in 2005, 2008, and 2014, respectively. His main field of research is constrained motion planning and control, particularly in the context of developing autonomous control and guidance algorithms for geometrically constrained aerospace systems.

Mehran Mesbahi received the Ph.D. degree from the University of Southern California, Los Angeles, in 1996. He was a member of the Guidance, Navigation, and Analysis group at the Jet Propulsion Laboratory, California, from 1996 to 2000 and an assistant professor of aerospace engineering and mechanics at the University of Minnesota from 2000 to 2002. He is currently a professor of Aeronautics and Astronautics, adjunct professor of Mathematics, and executive director of Joint Center for Aerospace Technology Innovation at the University of Washington (UW). He was the recipient of National Science Foundation CAREER Award in 2001, NASA Space Act Award in 2004, UW Distinguished Teaching Award in 2005, and UW College of Engineering Innovator Award for Teaching in 2008. His research interests are distributed and networked aerospace systems, systems and control theory, and engineering applications of optimization and combinatorics.